sustainability

MDPI

*Article*

# Greenhouse Gas Flux Responses and Regulating Pathways Under Combined Extreme Weather Events in Coastal Wetlands of the Yellow River Delta

**Xingcheng Hu [1], Chen Li [1], Qingxuan Meng [1], Guoliang Zhao [1], Zhengxi Cai [1], Qingliang Cui [2], Qingfeng Chen [1,†] and Lili Wang [1,*]**

[1] College of Geography and Environment, Shandong Normal University, Jinan 250014, China
[2] School of Resources and Environmental Engineering, Wuhan University of Technology, Wuhan 430070, China
* Correspondence: winni@sdnu.edu.cn
† Deceased author.

## Abstract

Compound extreme weather events are increasingly frequent due to global climate change; however, their impacts on greenhouse gas emissions from coastal wetlands and the associated biogeochemical pathways remain inadequately understood. In this study, we conducted laboratory incubation experiments utilizing soils from coastal wetlands in the Yellow River Delta, applying two combined extreme temperature–moisture treatments: extreme low-temperature drought (ELD) and extreme high-temperature flooding (EHF), alongside a control treatment (CK) under ambient temperature and moisture conditions. We measured $CO_2$, $CH_4$, and $N_2O$ fluxes, as well as soil carbon and nitrogen fractions, extracellular enzyme activities, and microbial community composition, to investigate the multilevel associative pathways that regulate greenhouse gas dynamics. The results indicated that ELD generally suppressed $CO_2$ and $CH_4$ emissions, with most habitats demonstrating net uptake or low emission rates; however, the reed habitat (RG) exhibited a transient $N_2O$ emission peak of 19.44 mg $m^{-2}$ $h^{-1}$ on day 7. EHF stimulated $CO_2$ emissions, with a peak flux of 22,407.23 mg $m^{-2}$ $h^{-1}$ recorded in the tidal flat (TF) on day 7, while $CH_4$ fluxes increased during the mid-incubation stage. EHF significantly diminished archaeal Chao1 richness and was associated with the enrichment of *Methanoculleus* (5% relative abundance) and *Nitrososphaeraceae*. In contrast, ELD led to the enrichment of Haloferax and *Candidatus Nitrosopumilus*. Partial least squares path modeling revealed that soil carbon and nitrogen fractions were indirectly linked to greenhouse gas emissions through the modulation of microbial community composition and extracellular enzyme activities. Soil organic carbon exhibited a positive correlation with bacterial communities, whereas carbon and nitrogen fractions were negatively correlated with archaeal communities. Fungal communities were closely associated with variations in $N_2O$ flux. These findings support a multilevel associative framework that connects extreme temperature–moisture regimes to greenhouse gas dynamics and provide a scientific foundation for evaluating carbon feedbacks and developing sustainable ecological management strategies for coastal wetlands in the context of climate change.

Academic Editor: Giuseppe Barbaro

Received: 28 October 2026
Revised: 20 November 2026
Accepted: 26 November 2026
Published: 29 November 2026

**Copyright:** © 2026 by the authors. Licensee MDPI, Basel, Switzerland. This article is an open access article distributed under the terms and conditions of the Creative Commons Attribution (CC BY) license.

**Keywords:** coastal wetlands; compound extreme weather events; greenhouse gas emissions; microbial communities; cascade effects

## 1. Introduction

Global warming has increased the frequency and intensity of extreme weather events worldwide, particularly heat extremes [1–4]. As summarised in the Sixth Assessment Report of the Intergovernmental Panel on Climate Change (IPCC AR6), warm days and nights have grown more frequent globally since the mid-20th century, with cascading impacts on ecosystem functioning, human health and food security [5–8]. Available records show that extreme heat frequency has more than tripled in recent decades relative to the mid-20th century baseline [9,10], and North China has experienced similarly pronounced increases in extreme temperatures and droughts alongside rising climatic variability [11]. Extreme weather events rarely occur in isolation; instead, they frequently manifest as compound extreme events, defined as multiple climatic hazards occurring simultaneously or sequentially that typically exert more severe impacts than individual events [12,13]. This concept was formalised in the IPCC Fifth Assessment Report and further elaborated in AR6, yet research to date has focused largely on meteorological characterisation and socioeconomic risk assessment. The ecological consequences of compound extremes, particularly their effects on soil biogeochemical cycling in vulnerable terrestrial ecosystems, remain far less understood.

Coastal wetlands are pivotal regulators of global carbon and nitrogen cycling and contribute substantially to the terrestrial greenhouse gas budget [14,15]. Situated at the land–ocean interface, these ecosystems are highly sensitive to shifts in temperature and hydrology, and their blue carbon functions are particularly susceptible to climate disturbances [16]. Considerable research has documented how individual climatic drivers, such as experimental warming, altered precipitation regimes and sea-level rise, modify greenhouse gas fluxes in coastal wetland soils [17,18]. Elevated temperature generally accelerates soil organic matter mineralisation and $CO_2$ efflux, whereas prolonged flooding creates anaerobic conditions that favour methanogenesis and $CH_4$ release. Nevertheless, most studies have evaluated the effects of single drivers independently. The response patterns of $CO_2$, $CH_4$ and $N_2O$ fluxes to coupled temperature and moisture extremes, and whether the magnitude and direction of response vary systematically across different wetland habitat types, remain poorly characterised. This knowledge gap constrains our ability to predict coastal wetland carbon feedbacks under intensifying climate extremes.

Soil greenhouse gas production and consumption are fundamentally microbially mediated processes, with extracellular enzymes catalysing the rate-limiting steps of organic matter decomposition and nutrient transformation [19,20]. Temperature and soil moisture jointly regulate these processes by modifying substrate availability, microbial community assembly and enzymatic reaction rates. Under warm, flooded conditions, for example, oxygen depletion selects for anaerobic functional groups such as methanogenic archaea and denitrifying bacteria, shifting carbon and nitrogen transformation pathways toward $CH_4$ and $N_2O$ production [21]. Under cold, dry conditions, by contrast, reduced substrate diffusion and constrained metabolic activity generally suppress microbial respiration and methanogenesis, though transient disruption of nitrogen transformation pathways can cause pulsed $N_2O$ emissions [22,23]. Despite these advances, most studies have examined microbial community composition or extracellular enzyme activities in isolation. Few have integrated soil substrate properties, microbial community structure, enzyme activities and gas fluxes into a single analytical framework, and the relative contributions of

these biotic and abiotic drivers to greenhouse gas dynamics under combined extreme temperature–moisture conditions remain unresolved.

Building on these findings, we designed this study to address two core research questions: first, how extreme low-temperature drought (ELD) and extreme high-temperature flooding (EHF) differentially affect soil $CO_2$, $CH_4$ and $N_2O$ fluxes, and whether responses vary across wetland habitat types; and second, what the relative contributions of soil carbon and nitrogen fractions, extracellular enzyme activities and microbial community shifts are in driving greenhouse gas flux responses. Based on established findings in wetland biogeochemistry and microbial ecology, we derived three testable hypotheses. First, the two combined extreme regimes would trigger divergent greenhouse gas responses: EHF would stimulate $CO_2$ and $CH_4$ emissions by accelerating organic matter mineralisation and creating anaerobic conditions, while ELD would generally suppress $CO_2$ and $CH_4$ fluxes via low-temperature inhibition of microbial metabolism and water limitation of substrate diffusion; $N_2O$ fluxes would exhibit transient emission peaks under both regimes due to imbalances in sequential nitrogen transformation steps, with response magnitudes differing across habitats. Second, soil carbon and nitrogen fractions would indirectly regulate greenhouse gas fluxes primarily by shaping microbial community composition and extracellular enzyme activities, rather than exerting strong direct effects, with archaea acting as key mediators of $CH_4$ dynamics and fungi being closely linked to $N_2O$ flux variation. Third, the coupling strength between soil substrates, microbial properties and greenhouse gas fluxes would differ between regimes, being stronger under EHF due to enhanced metabolic activity and substrate turnover, and weaker under ELD due to restricted substrate diffusion and suppressed microbial activity. To test these hypotheses, we conducted laboratory incubation experiments with soils from five typical habitat types in the Yellow River Delta coastal wetlands, combining measurements of greenhouse gas fluxes, soil carbon and nitrogen fractions, extracellular enzyme activities and bacterial, fungal and archaeal community composition. This study aims to characterise greenhouse gas flux responses to coupled extreme temperature–moisture regimes and disentangle the underlying microbial and biogeochemical mechanisms, providing a scientific basis for assessing carbon feedbacks and implementing sustainable ecological management of coastal wetlands under climate change.

## 2. Materials and Methods

### *2.1. Study Area and Sampling Design*

The Yellow River Delta (118°33′–119°21′ E, 37°35′–38°12′ N) is located in Dongying City, Shandong Province, China, and encompasses several administrative regions, including Hekou District, Kenli County, and Lijin County. The region has a warm-temperate, semi-humid continental monsoon climate, with hot, rainy summers and cold, dry winters. It is bordered by the Bohai Sea to the north and Laizhou Bay to the east. The mean annual temperature ranges from 11.7 to 12.3 °C, and annual precipitation ranges from 600 to 700 mm. During 1991–2020, the coastal wetlands of the Yellow River Delta experienced an annual average of 7.3 extreme heat days, 10.6 extreme cold days, 2.4 drought events, and 1.5 compound flood events. Long-term meteorological observations reveal significant alterations in temperature extremes within the Yellow River Delta. An analysis of daily data from five national meteorological stations in Dongying from 1994 to 2020 indicates that warm-temperature indices have generally increased, while cold-temperature indices have exhibited declining trends [24]. Furthermore, previous evaluations of precipitation records from these five stations have identified substantial interannual and seasonal variability, alongside an overall decreasing trend in annual and seasonal precipitation from 1961 to 2007 [25]. The region contains the Yellow River Delta National Nature Reserve, which protects recently formed estuarine wetlands that provide habitats for rare and

endangered bird species. These ecosystems are increasingly exposed to extreme weather events, including compound extremes that may affect regional ecological stability.

Soil samples were collected from five designated sites in the eastern Yellow River Delta: the Yellow River irrigation area (YA), tidal flat area (TF), reed habitat (RG), *Salicornia* habitat (EG), and *Apocynum* habitat (RR) (Figure 1). These sites were chosen through purposive sampling based on accessibility and habitat characteristics, rather than through random sampling. At each location, soil was extracted from a depth of 0–20 cm using the five-point sampling method. The soil samples collected from each site were pooled and thoroughly homogenized to create a composite soil sample at the site level. Each composite sample was then divided into aliquots for laboratory incubation, as well as for physicochemical and molecular analyses. For each site, three replicate incubation units were established for each treatment ($n$ = 3). Consequently, these three replicates represented within-site experimental replicates derived from the same composite soil sample, rather than independent field replicates. Given that only five purposively selected sites were included, these locations were treated as fixed sampling points, and the results were interpreted specifically for these sampled sites rather than as representative of all coastal wetlands in the Yellow River Delta.

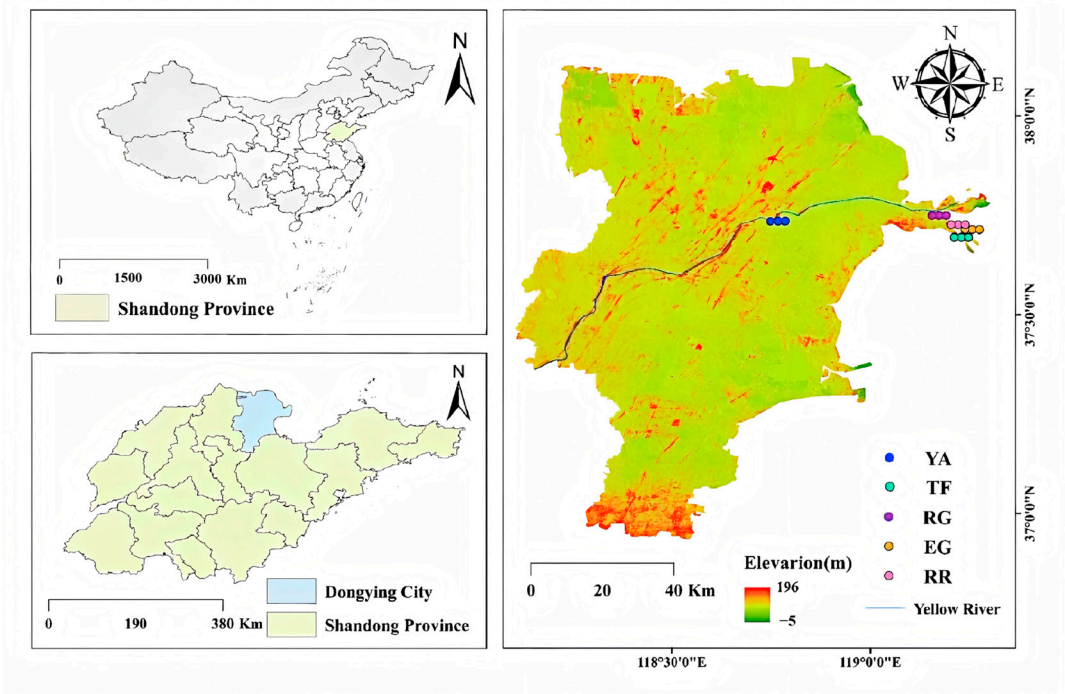



**Figure 1.** Sampling sites of typical vegetation in coastal wetlands of the Yellow River Delta. Note: YA is river irrigation area land, TF is tidal flat area land, RG is reed habitat land, EG is *Salicornia* habitat land, and RR is *Apocynum* habitat land.

### *2.2. Experimental Design and Laboratory Incubation*

After being transported to the laboratory, plant roots, sand, stones, and other visible impurities were removed from the soil samples. The soil was air-dried and transferred to serum vials. Distilled water was added based on the soil moisture conditions at the sampling sites, and the samples were placed in incubators under different temperature and moisture regimes to simulate compound extreme weather events. Three treatments were established as follows: a control (CK), maintained at 25 °C and a soil water content (SWC) of 25%; extreme low-temperature drought (ELD), maintained at −19 °C and 5% SWC; and extreme high-temperature flooding (EHF), maintained at 45 °C and 50% SWC, which were displayed in Table 1. The experimental design comprised solely three treatment

combinations and excluded treatments involving low temperature, drought, high temperature, or flooding in isolation. Consequently, it was not a full factorial design, limiting the ability to estimate the independent effects of temperature and moisture, as well as their interactions. This experiment aimed to compare soil responses to these predefined combinations against a control, rather than to characterize the frequency, duration, sequence, lag, or co-occurrence probability of natural compound events.

**Table 1.** Experimental treatments and corresponding incubation conditions.

| Treatment | Temperature | SWC | Description |
|---|---|---|---|
| CK | 25 °C | 25% | Control |
| ELD | −19 °C | 5% | Combined low-temperature and low-moisture treatment |
| EHF | 45 °C | 50% | Combined high-temperature and high-moisture treatment |

Note: Each treatment was applied to soils from all five selected habitat types, with three incubation replicates per habitat × treatment combination, if confirmed by the experimental records.

### *2.3. Test Parameters and Methods*

#### 2.3.1. Determination of Soil Carbon and Nitrogen Fractions and Moisture Content

Soil Organic Carbon (SOC) was determined using the potassium dichromate volumetric and titration method. Ammonium nitrogen ($NH_4^+$), nitrate nitrogen ($NO_3^-$), and nitrite nitrogen ($NO_2^-$) were determined using an AA3 continuous-flow analyzer (Seal Analytical GmbH, Norderstedt, Germany) after extracted with 2 mol $L^{-1}$ KCl solution by shaking. Soil moisture content (SWC) was determined gravimetrically using the oven-drying method. SWC was calculated as follows:

$$SWC(\%) = \frac{m_{wet} - m_{dry}}{m_{dry}} \times 100 \quad (1)$$

where $m_{wet}$ is the mass of the fresh soil sample (g), and $m_{dry}$ is the mass of the soil sample after oven-drying at 105 °C to constant mass (g).

#### 2.3.2. Measurement of Soil Greenhouse Gas Fluxes

Soil $CO_2$, $CH_4$, and $N_2O$ fluxes were measured using the static-chamber method under varying temperature and moisture treatments. Gas samples were collected on days 1, 3, 5, 7, and 14 of the incubation period. On each sampling day, gas samples were withdrawn from the serum vials through the sampling ports at 0, 15, 30, and 45 min using a 20 mL gas-tight syringe. Prior to each sample collection, a gas volume equivalent to twice the syringe capacity was drawn through the syringe for purging. The collected samples were transferred to 12 mL evacuated glass vials that had been flushed with helium. $CO_2$, $CH_4$, and $N_2O$ concentrations were determined within 24 h using a gas chromatograph (Agilent 7890B, Inc., Santa Clara, CA, USA). Gas sampling was conducted repeatedly using the same incubation units throughout the experimental period, enabling the evaluation of temporal changes in GHG fluxes for each experimental unit.

The greenhouse gas (GHG) fluxes were calculated from the linear regression of gas concentration against sampling time. Measurements with regression coefficients of determination ($R^2$) below 0.9 were excluded. GHG fluxes (mg $m^{-2}$ $h^{-1}$) were calculated as follows:

$$GHG_{flux} = \frac{dc}{dt} \cdot \frac{M}{v_0} \cdot \frac{p}{p_0} \cdot \frac{T_0}{T} \cdot H \quad (2)$$

where $dc/dt$ represents the rate of change in gas concentration during sampling, $M$ is the molar mass of the target gas, $p$ is the atmospheric pressure at the sampling site, $T$ is the absolute temperature inside the static chamber, $V_0$, $p_0$ and $T_0$ refer to the molar volume of

gas, atmospheric pressure and absolute temperature under standard conditions, respectively, and H is the height of the chamber above the water surface.

The global warming potential (*GWP*) of greenhouse gas emissions under each treatment was estimated using Equation (3) and expressed in mg $CO_2$-eq $m^{-2}$ $h^{-1}$.

$$GWP = CO_2 + 29.8 \times CH_4 + 273 \times N_2O \quad (3)$$

2.3.3. Determination of Soil Extracellular Enzyme Activities

Soil extracellular enzyme activities were determined to assess enzyme responses associated with carbon and nitrogen transformations [19]. Cellulase activity was determined using the nitrosalicylic acid colorimetric method, and sucrase activity was measured using the 3,5-dinitrosalicylic acid colorimetric method [20]. Polyphenol oxidase and protease activities were determined using colorimetric methods. β-1,4-N-acetylglucosaminidase activity was determined using the p-nitrophenol colorimetric method. Catalase activity was measured using potassium permanganate titration, whereas ammonia monooxygenase activity was determined using an enzyme-linked immunosorbent assay (ELISA) [26]. Nitrate reductase activity was measured using the phenylenedisulfonic acid colorimetric method. Nitric oxide reductase and nitrous oxide reductase activities were determined from gas production rates, and urease activity was measured using the sodium phenolate–sodium hypochlorite colorimetric method [27].

2.3.4. Soil DNA Extraction and High-Throughput Sequencing

Approximately 0.2–0.5 g of soil was transferred to a centrifuge tube containing extraction lysis buffer, and the sample was homogenized by grinding. Soil DNA was extracted using an OMEGA Soil DNA Kit (D5635-02; Omega Bio-Tek, Norcross, GA, USA). DNA integrity was assessed by electrophoresis on a 0.8% agarose gel, and DNA concentration was measured using a NanoDrop 2000 spectrophotometer (Thermo Fisher Scientific, Wilmington, DE, USA) [28].

The bacterial 16S rRNA gene V3–V4 region, the fungal internal transcribed spacer 1 (ITS1) region, and the archaeal 16S rRNA gene V4–V5 region were amplified for high-throughput sequencing. For archaeal community profiling, the V4–V5 region was amplified using the primer pair 524F (5′-TGYCAGCCGCCGCGGTAA-3′) and 958R (5′-YCCGGCGTTGAVTCCAATT-3′), with a sample-specific 7–10 bp barcode incorporated at the 5′ end of the forward primer. While the V4–V5 region is also utilized in bacterial 16S rRNA gene studies, its application is not limited to bacteria; the taxonomic specificity of amplification is primarily determined by the primer sequences. The reverse primer 958R corresponds to Arch958R-mod, which was assessed for archaeal specificity using the Ribosomal Database Project (RDP) database, demonstrating significantly higher alignment with archaeal sequences compared to bacterial sequences [29]. The 524F/958R primer pair has been employed in prior studies to characterize archaeal communities in soil environments [30]. PCR amplification was conducted utilizing Q5 high-fidelity DNA polymerase (New England Biolabs, Ipswich, MA, USA) under the following parameters: an initial denaturation at 98 °C for 5 min, succeeded by 35 cycles comprising denaturation at 98 °C for 30 s, annealing at 65 °C for 30 s, and extension at 72 °C for 45 s, culminating in a final extension at 72 °C for 5 min. The resulting amplification products were resolved by electrophoresis on a 2% agarose gel. Target bands were excised, and the DNA fragments were purified employing an Axygen Gel Recovery Kit. Sequencing libraries were constructed using a TruSeq Nano DNA Library Prep Kit. Library concentrations were assessed with a Quant-iT PicoGreen dsDNA Assay Kit in conjunction with a Promega QuantiFluor instrument. Following quality control, the libraries were sequenced on an Illumina NovaSeq 6000 platform (Illumina, Inc., San Diego, CA, USA) [31].

### *2.4. Data Processing and Statistical Analysis*

Statistical analyses were performed using IBM SPSS Statistics (version 27.0) and Microsoft Excel (version 2016). Differences among treatments were evaluated using one-way analysis of variance (ANOVA), followed by the least significant difference (LSD) test. Statistical significance was assessed at the level of 0.01, 0.05, and 0.001. Pearson correlation analyses were performed, and correlation heatmaps were generated using R (version 4.2.2). Redundancy analysis (RDA) of soil environmental factors and functional genes was performed using Canoco 5.0. High-throughput sequencing data were analyzed using the Novomagic cloud platform (version V3.0, Novogene, Beijing, China). Differential analyses of microbial community data were performed using the online visualization platform ChiPlot (https://www.chiplot.online).

Mantel tests were performed via R 4.2.2to examine pairwise associations between soil biogeochemical properties, enzyme activities, and GHG fluxes (GWP), and to compare the strength of these couplings under ELD and EHF treatments. LEfSe analysis was conducted to screen microbial taxa differing markedly in abundance among treatments and identify biomarker taxa that responded specifically to each compound extreme treatment. Partial least squares path modeling (PLS-PM) was applied to disentangle direct and indirect pathways, quantifying how temperature and soil moisture conditions shape greenhouse gas emissions sequentially through soil carbon and nitrogen substrates, microbial communities and extracellular enzyme activities.

## 3. Results

### *3.1. The Effects of Compound Extreme Weather Events on Greenhouse Gas Flux*

#### 3.1.1. Greenhouse Gas Fluxes Under ELD

Under ELD condition, $CO_2$, $CH_4$, and $N_2O$ fluxes were generally lower, although transient emission peaks were observed at several sites (Figure 2a). On day 1, $N_2O$ fluxes were predominantly negative (−2.88 to −2.24 mg $m^{-2}$ $h^{-1}$), with RR showing a slightly positive flux. $CH_4$ uptake was observed at YA, RG, and EG. $CO_2$ fluxes were negative at YA and RG, whereas RR exhibited low positive emissions (990.73 ± 9.33 mg $m^{-2}$ $h^{-1}$). During days 3–7, gas fluxes fluctuated but generally remained low. At YA, $N_2O$ flux reached 11.23 mg $m^{-2}$ $h^{-1}$ on day 3 before declining rapidly, whereas TF showed a minimum of −26.03 mg $m^{-2}$ $h^{-1}$ on day 5. $CH_4$ fluxes remained low, with TF reaching a minimum of −3.12 mg $m^{-2}$ $h^{-1}$ on day 7. $CO_2$ fluxes became positive at some sites on day 3 before declining again. At RG, $N_2O$ flux peaked at 19.44 mg $m^{-2}$ $h^{-1}$ on day 7, the highest value recorded under ELD. During the later incubation period, $N_2O$ fluxes declined close to zero, $CH_4$ fluxes fluctuated slightly, and $CO_2$ fluxes remained predominantly negative. Overall, ELD was associated with low $CO_2$ and $CH_4$ fluxes, whereas $N_2O$ showed greater temporal variability, including transient emission peaks.

#### 3.1.2. Greenhouse Gas Fluxes Under EHF

Under EHF, greenhouse gas fluxes generally increased during the early and middle stages of incubation, and then decreased by the late incubation stage (Figure 2b). During the early incubation stage, $N_2O$ fluxes were mostly positive, and emissions were comparatively high at RR, RG and EG. $CH_4$ fluxes were generally low, with positive emissions observed only at RR and EG. $CO_2$ emissions were elevated at the beginning of incubation, reaching 10,289.01 mg $m^{-2}$ $h^{-1}$ at RR, while values at the remaining sites ranged from 4000 to 7000 mg $m^{-2}$ $h^{-1}$. During the middle stage, $N_2O$ fluxes at RG and TF reached 6.28 and 8.98 mg $m^{-2}$ $h^{-1}$ on days 5 and 7, respectively. $CH_4$ fluxes increased, becoming positive at most sites, with TF reaching 0.76 mg $m^{-2}$ $h^{-1}$ on day 7. The highest $CO_2$ flux was recorded at TF on day 7 (22,407.23 mg $m^{-2}$ $h^{-1}$). Toward the end of incubation, $N_2O$ fluxes became

negative at some sites, while $CH_4$ fluxes declined to approximately zero. $CO_2$ fluxes stayed positive at YA and TF, whereas RG, EG and RR showed negative values. Overall, EHF was associated with elevated $CO_2$ and $N_2O$ emissions during the middle incubation period, while the increase in $CH_4$ fluxes were comparatively limited. $CO_2$ fluxes increased rapidly and then declined afterward.

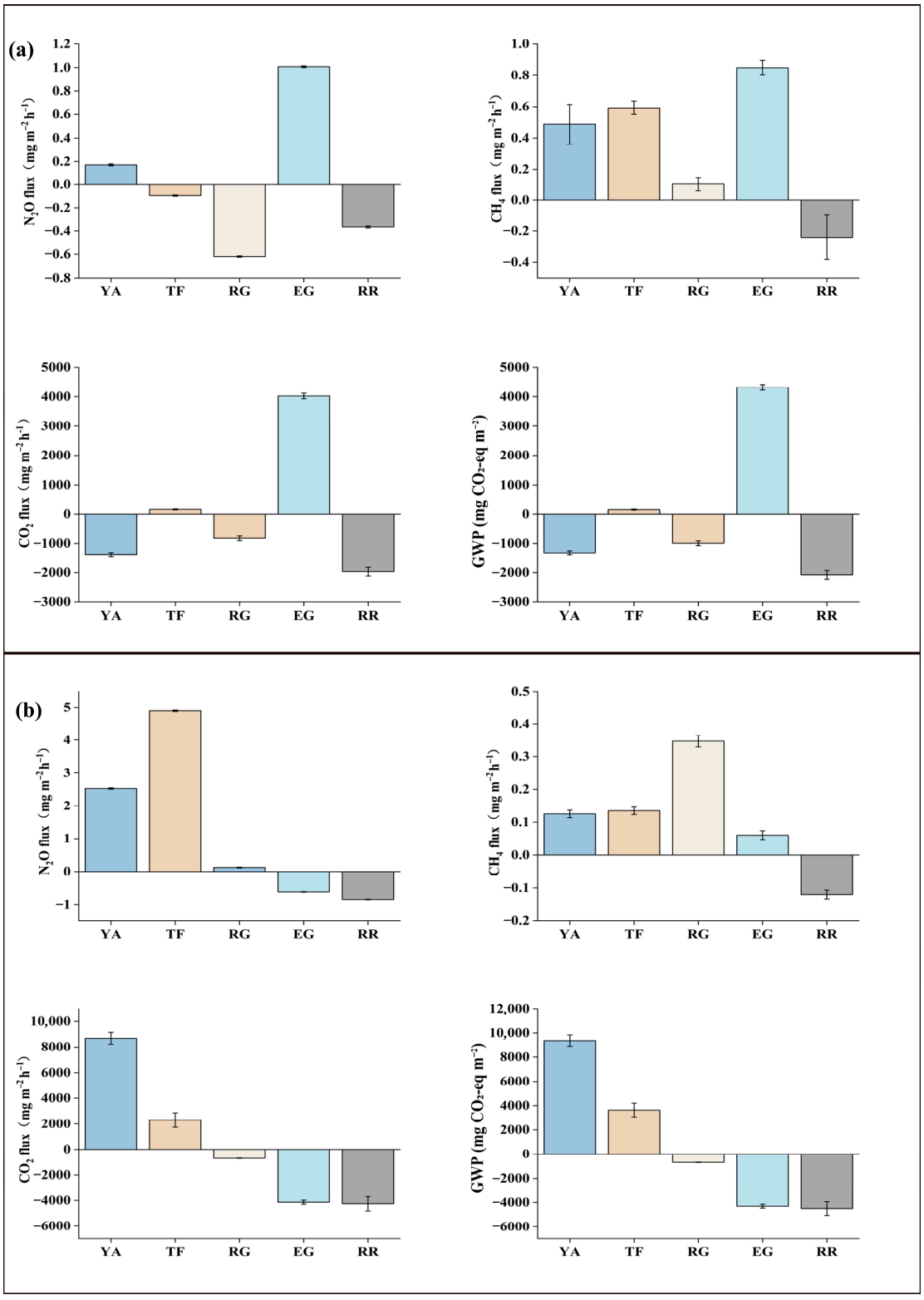



**Figure 2.** Greenhouse gas fluxes from Yellow River Delta coastal wetland soils under (**a**) ELD and (**b**) EHF. Note: Mean greenhouse gas fluxes and global warming potential (GWP) across the five sampling sites under (**a**) ELD and (**b**) EHF treatments. For each incubation unit, GHG fluxes

measured on days 1, 3, 5, 7, and 14 were averaged to obtain the mean flux across the five sampling dates. Bars represent the means of three incubation replicates. YA, Yellow River irrigation area; TF, tidal flat; RG, reed habitat; EG, *Salicornia* habitat; RR, *Apocynum* habitat.

### *3.2. The Impact of Compound Extreme Weather Events on Soil Carbon and Nitrogen Components*

Under ELD, SOC concentrations were generally higher than those under CK and remained relatively high throughout incubation (Figure 3a). On day 7, SOC concentrations ranged from 5.52 to 6.35 g $kg^{-1}$. Ammonium nitrogen ($NH_4^+$) concentrations were generally lower than those under CK and showed limited temporal variation, ranging from 0.24 to 1.14 mg $L^{-1}$ on day 7. In contrast, nitrate nitrogen ($NO_3^-$) concentrations were higher than those under CK, reaching 13.99–26.11 mg $L^{-1}$ on day 3. Under EHF, SOC concentrations were generally lower than those under CK and declined during incubation (Figure 3b). On day 14, SOC concentrations ranged from 5.42 to 7.60 g $kg^{-1}$. $NH_4^+$ concentrations increased during the early incubation period, reaching 2.97–5.91 mg $L^{-1}$ on day 3. $NO_3^-$ concentrations initially increased and subsequently declined. The two treatments showed contrasting patterns in soil carbon and nitrogen fractions. ELD was associated with relatively high SOC and $NO_3^-$ concentrations and lower $NH_4^+$ concentrations, whereas EHF was associated with declining SOC concentrations, elevated $NH_4^+$ concentrations during early incubation, and an initial increase followed by a decrease in $NO_3^-$ concentrations.

### *3.3. The Effects of Compound Extreme Weather Events on Enzyme Activities*

Soil enzyme activities differed between ELD and EHF treatments and among sampling sites (Figure 4). Under ELD, nitric oxide reductase (NOR) activity at YA decreased from 104.087 to 13.294 U $g^{-1}$, a reduction of 90.793 U $g^{-1}$ and the largest decrease among the sampling sites. At EG, NOR activity decreased from 36.125 to 20.563 U $g^{-1}$, a reduction of 15.562 U $g^{-1}$. In contrast, nitrous oxide reductase ($N_2OR$) activity at RR increased to 23.487 U $g^{-1}$, exceeding the CK value by 14.256 U $g^{-1}$ and representing the largest increase among sites. Sucrase activity at TF increased from 128.140 to 152.349 U $g^{-1}$, an increase of 24.209 U $g^{-1}$. Under EHF, several nitrogen-cycling enzymes showed greater increases in activity than under the other treatments. $N_2OR$ activity at TF reached 67.769 U $g^{-1}$, the highest value among all treatments. At EG, $N_2OR$ activity increased from 2.308 to 48.077 U $g^{-1}$, an increase of 45.769 U $g^{-1}$, while nitrate reductase (NR) activity reached 46.125 U $g^{-1}$. At RR, protease activity increased to 112.923 U $g^{-1}$, exceeding the CK value by 65.034 U $g^{-1}$. In contrast, NOR activity at YA decreased to 18.254 U $g^{-1}$, a reduction of 85.833 U $g^{-1}$ relative to CK.

### *3.4. The Effects of Compound Extreme Weather Events on Soil Microbial Communities*

#### 3.4.1. Microbial $\alpha$-Diversity and $\beta$-Diversity

Bacterial $\alpha$-diversity differed among treatments (Figure 5(a1)). The Chao1 richness index showed a significant treatment effect ($p < 0.01$). Compared with CK, bacterial richness was lower under EHF and relatively higher under ELD. Significant differences were also observed in the Simpson, Pielou's evenness, and Shannon indices, although changes in evenness and overall diversity were relatively small. Principal coordinates analysis (PCoA) showed that PC1 and PC2 explained 18.6% and 13.6% of the variation in bacterial community composition, respectively, accounting for a cumulative 32.2% (Figure 5(a2)). Samples from the ELD and EHF treatments occupied distinct regions of the ordination, while CK samples were distributed toward the opposite side. Some overlap remained among treatment groups.

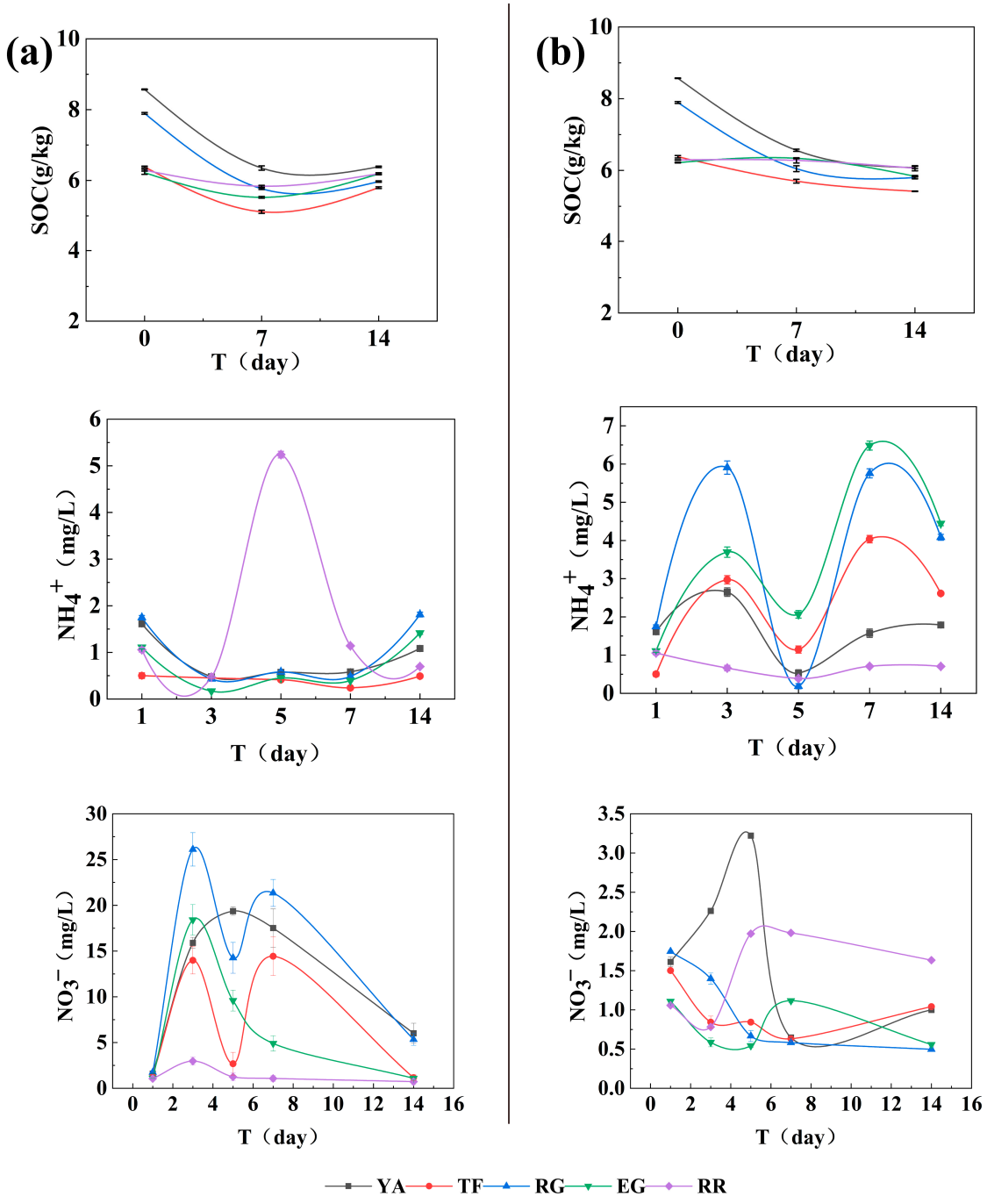



**Figure 3.** Temporal changes in soil SOC, $NH_4^+$, and $NO_3^-$ concentrations under (**a**) ELD and (**b**) EHF. Note: YA is river irrigation area land, TF is tidal flat area land, RG is reed habitat land, EG is *Salicornia* habitat land, and RR is *Apocynum* habitat land.

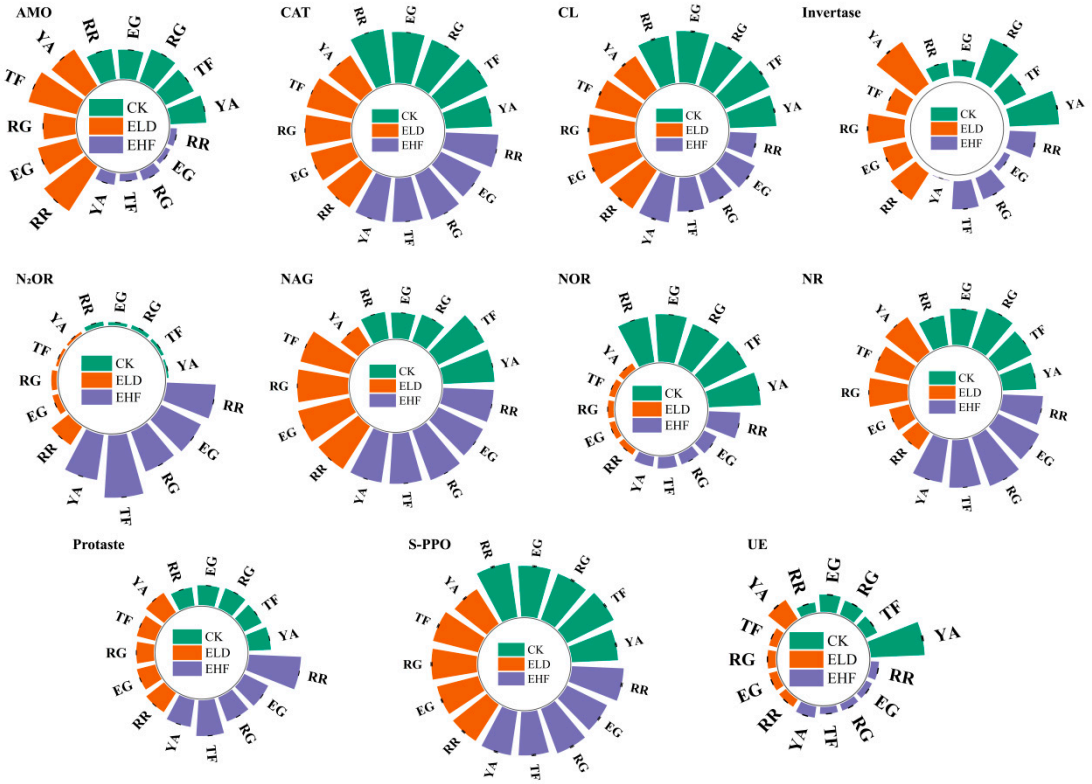



**Figure 4.** Characteristics of soil enzyme activity changes under compound extreme weather conditions. Note: YA is river irrigation area land, TF is tidal flat area land, RG is reed habitat land, EG is *Salicornia* habitat land, and RR is *Apocynum* habitat land. CK is control, ELD is extreme low-temperature drought, and EHF is extreme high-temperature flooding.

Fungal $\alpha$-diversity also differed among treatments (Figure 5(b1)). The Chao1 index showed significant differences ($p < 0.01$), with lower richness under EHF than under CK, while ELD showed a variable response. Significant differences were observed in the Shannon ($p < 0.05$) and Pielou's evenness ($p < 0.05$) indices, whereas the Simpson index did not differ significantly. Fungal richness and diversity were generally lower under EHF. In the fungal PCoA, PC1 and PC2 explained 6.2% and 5.3% of the variation, respectively, accounting for a cumulative 11.5% (Figure 5(b2)). ELD and EHF samples showed some separation from CK samples, although substantial overlap was observed among the three treatment groups.

Archaeal $\alpha$-diversity indices differed significantly among treatments (Figure 5(c1)). The Chao1, Simpson, Pielou's evenness, and Shannon indices all showed values of p less than 0.01. CK samples showed the highest richness, evenness, and overall diversity. All four indices were lower under EHF, whereas ELD generally showed intermediate values. Archaeal PCoA showed that PC1 and PC2 explained 20.3% and 14.6% of the variation in community composition, respectively, accounting for a cumulative 34.9% (Figure 5(c2)). The three treatment groups showed a gradient along PC1, with CK samples concentrated toward the negative axis, ELD samples occupying an intermediate position, and EHF samples distributed toward the positive axis. The groups showed distinct clustering patterns, although their distributions overlapped.

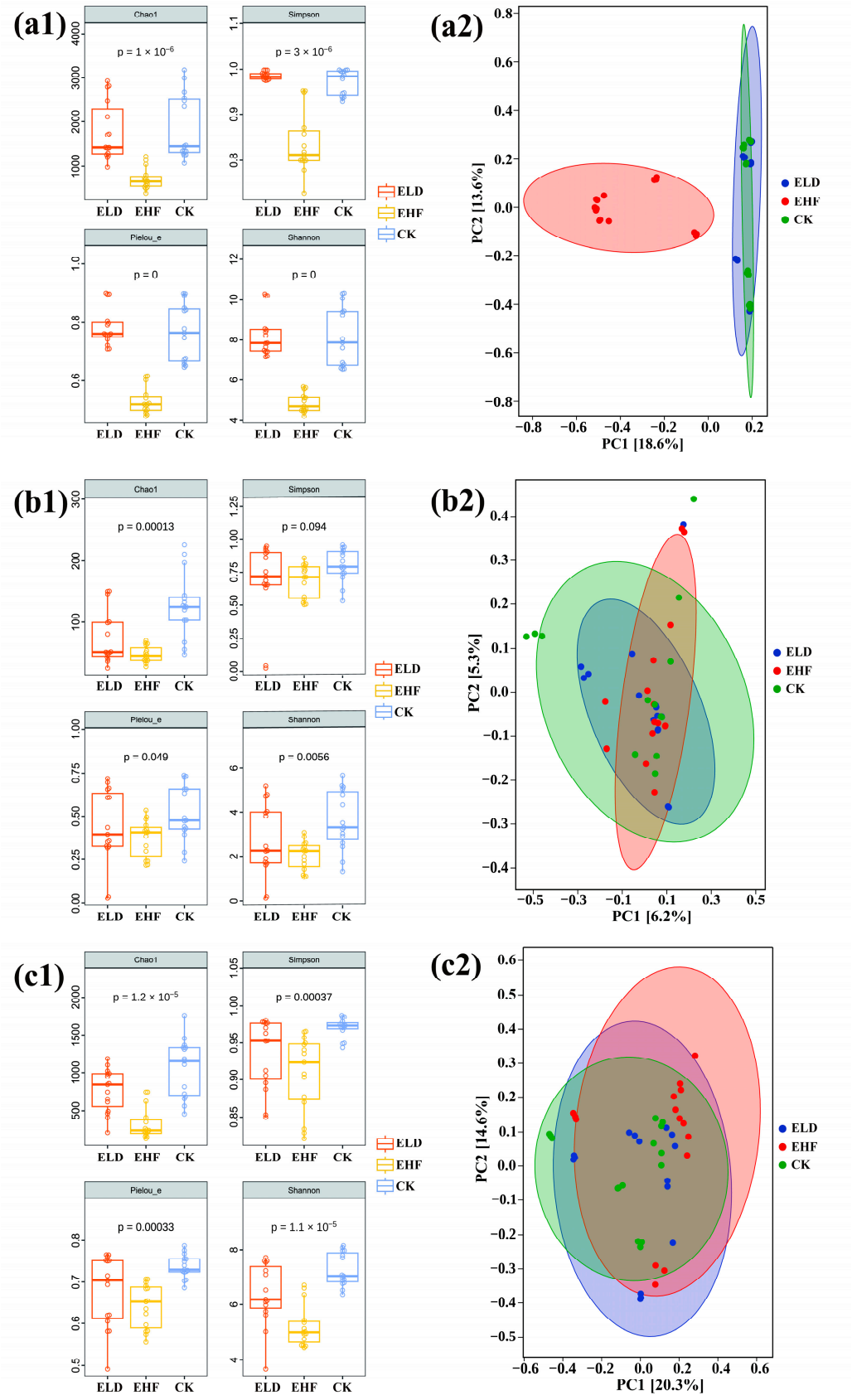



**Figure 5.** Characteristics of soil microbial communities under compound extreme weather conditions. Note: (**a1**) Alpha diversity of soil bacterial communities under compound extreme weather conditions; (**a2**) PCoA plot of beta diversity indices for soil bacteria based on OTU levels under compound extreme weather conditions; (**b1**) Alpha diversity off soil fungal communities under

compound extreme weather conditions; (**b2**) PCoA plot of beta diversity indices for soil fungi based on OTU levels under compound extreme weather conditions; (**c1**) Alpha diversity of soil archaea communities under compound extreme weather conditions; (**c2**) PCoA plot of beta diversity indices for soil archaea based on OTU levels under compound extreme weather conditions. In panels (**a2**), (**b2**), and (**c2**), each point represents an individual sample, and the shaded ellipses illustrate the spread of samples within each treatment group (purple for ELD, orange for EHF, and green for CK). CK is control, ELD is extreme low-temperature drought, and EHF is extreme high-temperature flooding.

### 3.4.2. Differential Indicator Groups and Key Functional Microorganisms

Bacterial communities. Linear discriminant analysis effect size (LEfSe) analysis identified differentially enriched bacterial taxa among treatments using a linear discriminant analysis (LDA) threshold of 2 (Figure 6(a1,a2)). The taxonomic cladogram showed the distribution of differentially enriched groups (Figure 6(a1)), while LDA scores identified characteristic taxa associated with each treatment (Figure 6(a2)). Under ELD, *Salinimicrobium*, *Alcanivorax*, and *Pseudomonas* were significantly enriched. The EHF treatment was characterized by enrichment of *Rhodococcus* and *Azospirillum*. Under CK, *Longimicrobiaceae* and BD2-11_terrestrial_group were among the enriched taxa.

Fungal communities. LEfSe analysis identified distinct fungal indicator taxa among treatments at an LDA threshold of 2 (Figure 6(b1,b2)). The cladogram showed the taxonomic distribution of differentially enriched groups (Figure 6(b1)), while the LDA scores quantified their discriminatory contributions (Figure 6(b2)). Under ELD, *Postia*, *Aureobasidium*, and *Alternaria* showed the highest enrichment. Under EHF, *Aspergillus*, *Squamarina*, and *Cercospora* were the main differentially enriched genera. Under CK, *Tuber*, *Geosmithia*, and *Sollicozyma* were the dominant indicator taxa.

Archaeal communities. LEfSe analysis identified differentially enriched archaeal taxa among treatments using an LDA threshold greater than 2 (Figure 6(c1,c2)). The cladogram showed their taxonomic distribution (Figure 6(c1)), and the LDA scores identified the taxa most strongly associated with each treatment (Figure 6(c2)). Under ELD, *Haloferax* and *Candidatus Nitrosopumilus* were significantly enriched. Under EHF, *Nitrososphaeraceae* and *Methanoculleus* showed the highest enrichment, with the relative abundance of *Methanoculleus* reaching 5%. Under CK, *Candidatus Nitrocosmicus*, *Halolamina*, and *Halomicroarcula* were enriched.

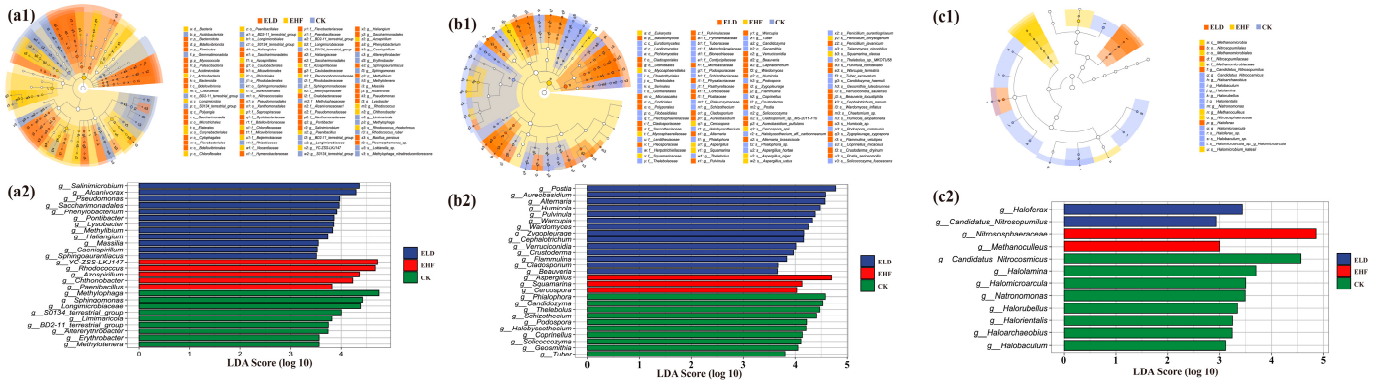



**Figure 6.** LEfSe analysis of soil microbial communities under compound extreme weather conditions. Note: (**a1**,**a2**) soil bacterial microbial communities; (**b1**,**b2**) soil fungal microbial communities; (**c1**,**c2**) soil archaea microbial communities.

### *3.5. Relationships Among Soil Properties, Microorganisms, and Greenhouse Gas Emissions*

#### 3.5.1. Associations Between Soil Properties and Greenhouse Gas Fluxes

Mantel tests showed differences in the associations between soil properties, enzyme activities, and greenhouse gas emission indicators under ELD and EHF (Figure 7a,b). Under ELD, SOC, $NH_4^+$, and $NO_3^-$ generally showed weak associations with $CO_2$, $CH_4$, and $N_2O$ fluxes and global warming potential (GWP) (Figure 7a). Among the soil carbon and nitrogen fractions, only SOC was significantly positively correlated with $CO_2$ flux. Among carbon-cycling enzymes, cellulase (CL) showed a significant positive correlation with GWP ($p < 0.01$), whereas invertase and β-1,4-N-acetylglucosaminidase (NAG) showed moderate positive correlations with $CO_2$ flux. Associations between nitrogen-cycling enzymes (NR, ammonia monooxygenase (AMO), and $N_2OR$) and emission indicators were generally not statistically significant. Under EHF, stronger associations were observed between soil properties, enzyme activities, and greenhouse gas fluxes (Figure 7b). SOC was significantly positively correlated with $CO_2$ flux and GWP ($p < 0.001$), while all measured inorganic nitrogen fractions showed significant correlations with $N_2O$ flux. Carbon-cycling enzymes showed moderately strong correlations with $CO_2$ flux. NR, AMO, and $N_2OR$ showed significant positive correlations with GWP ($p < 0.001$).

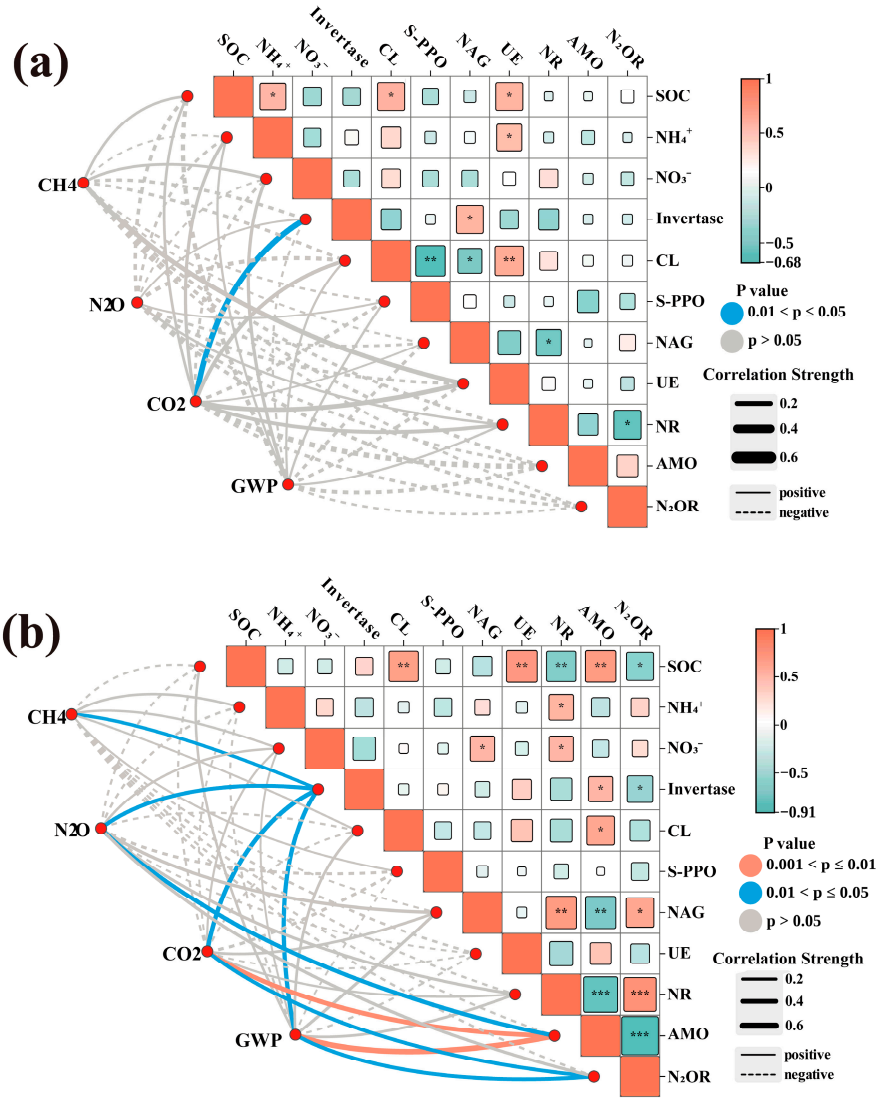


**Figure 7.** Correlations between greenhouse gas fluxes and soil environmental factors under compound extreme weather conditions. Note: (**a**) extreme low temperature and drought (ELD); (**b**) extreme high temperature and flooding (EHF). * $p < 0.05$, ** $p < 0.01$, and *** $p < 0.001$.

### 3.5.2. Key Environmental Drivers of Microbial Community Structure

Redundancy analysis (RDA) showed associations between microbial community composition and temperature (T), SWC, and SOC (Figure 8a–c). For bacterial communities, the first two RDA axes explained 30.05% of the variation, with Axis 1 and Axis 2 accounting for 18.05% and 12.05%, respectively (Figure 8a). *Chthonobacter* and *Azospirillum* were positively associated with temperature, SWC, and soil nitrogen, whereas *Rhodococcus* was negatively associated with SOC. For fungal communities, the first two axes explained 13.78% of the variation, with Axis 1 accounting for 7.48% and Axis 2 for 6.30% (Figure 8b). *Chaetomium* and *Fusarium* were positively associated with environmental factors, whereas *Postia* and *Humicola* showed negative associations. For archaeal communities, the first two axes explained 20.25% of the variation, with Axis 1 and Axis 2 accounting for 11.73% and 8.52%, respectively (Figure 8c). *Nitrososphaeraceae* and *Candidatus Nitrocosmicus* were positively associated with temperature, SWC, and SOC, whereas halophilic archaea, including *Halogranum*, showed negative associations. The first two RDA axes accounted for 30.05% of the variation in bacterial communities, 13.78% in fungal communities, and 20.25% in archaeal communities. These findings suggest that the assessed environmental variables explained only a portion of the overall variation in microbial community composition, especially for fungi. Consequently, the identified ordination patterns should be regarded as associations with the measured environmental factors rather than as complete explanations of microbial community assembly.

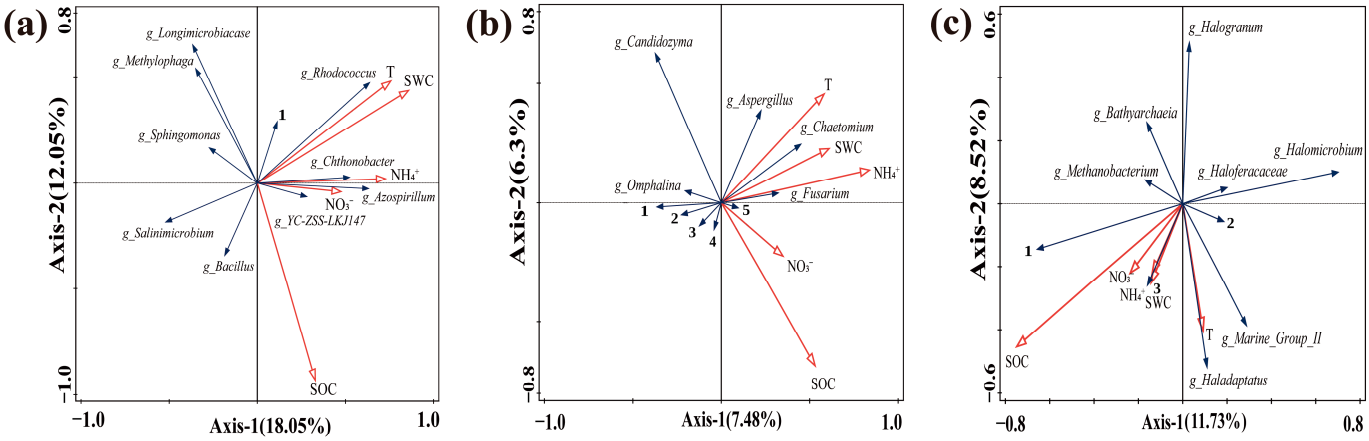



**Figure 8.** Redundancy analysis (RDA) of microbial communities and environmental variables under compound extreme weather conditions. Note: (**a**) Bacteria, (**b**) Fungi, (**c**) Archaea.

### 3.5.3. A Multi-Level Pathway Linking for Greenhouse Gas Emissions

Partial least squares path modeling (PLS-PM) served as an exploratory method to investigate the relationships among temperature, soil water content (SWC), soil carbon and nitrogen fractions, microbial communities, extracellular enzyme activities, and greenhouse gas emissions (Figure 9). The model produced a goodness-of-fit (GoF) value of 0.37. Temperature and SWC were identified as upstream predictors influencing changes in soil carbon and nitrogen fractions. Soil organic carbon (SOC) exhibited a positive association with bacterial communities (path coefficient = 0.56; $R^2$ = 0.47), whereas soil nitrogen

demonstrated a positive relationship with fungal communities (path coefficient = 0.64; $R^2$ = 0.40). Conversely, SOC and soil nitrogen were negatively correlated with archaeal communities, with path coefficients of −0.82 and −0.41, respectively ($R^2$ = 0.71). Bacterial communities displayed a negative association with carbon-cycling enzymes (path coefficient = −0.41; $R^2$ = 0.69). Regarding nitrogen-cycling enzymes, bacterial and fungal communities exhibited path coefficients of −0.69 and 0.41, respectively ($R^2$ = 0.84). The model accounted for 32%, 35%, and 29% of the variation in $N_2O$, $CH_4$, and $CO_2$ emissions, respectively ($R^2$ = 0.32, 0.35, and 0.29). The explanatory power of the model varied across endogenous constructs, revealing relatively low $R^2$ values for greenhouse gas emissions. Specifically, the model explained less than 35% of the variation in each of the three greenhouse gases, suggesting that additional factors not included in the model may influence their emission patterns. The GoF value of 0.37 serves as a descriptive index and should not be regarded as independent evidence of sufficient model specification. Moreover, the estimated path coefficients reflect associations within the specified model rather than direct evidence of causal or temporally ordered relationships. Consequently, the PLS-PM results should be viewed as exploratory evidence of potential linkages among soil properties, microbial communities, enzyme activities, and greenhouse gas emissions.

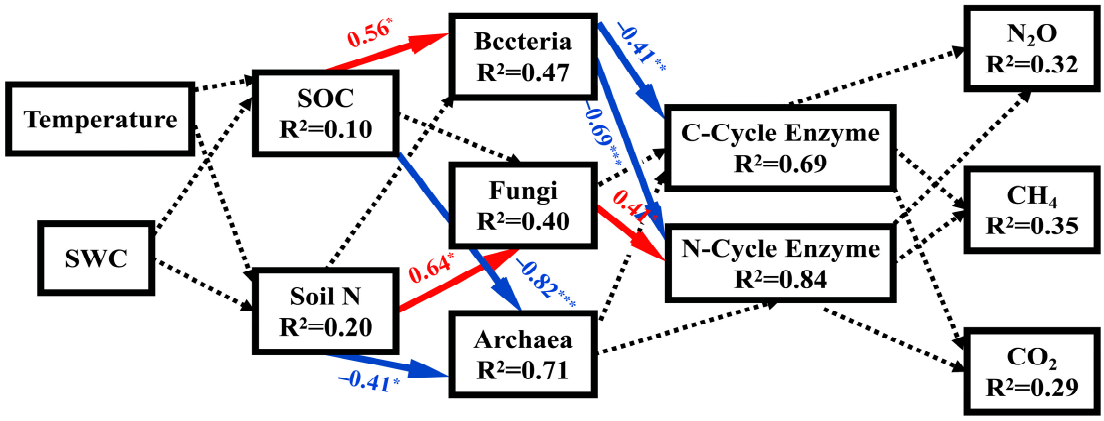



**Figure 9.** Partial least squares path model (PLS-PM) for multi-pathway regulation of greenhouse gas emissions. Note: *N* = 45 samples, GOF = 0.37, SRMR = 0.08. * $p < 0.05$, ** $p < 0.01$, and *** $p < 0.001$.

## 4. Discussion

### *4.1. Responses of Greenhouse Gas Emissions Under Compound Extreme Weather Conditions*

Previous studies have investigated the effects of individual climatic extremes on carbon and nitrogen cycling in wetlands [17]. Temperature and moisture extremes may co-occur in natural environments, and their combined effects could vary based on the intensity of each factor and local soil conditions [16,32,33]. However, the current experiment, which included only the control and two combined treatments, cannot ascertain whether the observed responses were additive or interactive, nor can it isolate the individual contributions of temperature and moisture. Consequently, the following discussion emphasizes the differing soil responses noted under the two specified temperature–moisture combinations. Low temperatures may constrain enzymatic reactions, while water limitation reduces substrate diffusion and microbial activity [34–37]. These constraints may explain the generally low $CO_2$ and $CH_4$ fluxes under ELD. Transient $N_2O$ emissions could be associated with changes in substrate availability or microbial nitrogen transformations during environmental fluctuations, although freeze–thaw or wetting–drying processes were not directly examined [23].

In contrast, EHF was associated with increased $CO_2$ emissions and an increase in $CH_4$ fluxes during the middle stage of incubation (Figure 2b). Higher temperatures may accelerate organic matter mineralization, while flooding can restrict oxygen diffusion and create reducing conditions that favor anaerobic microbial processes [21,38,39]. These processes may have contributed to the observed emission peaks and subsequent declines. The differing responses observed under ELD and EHF suggest that greenhouse gas fluxes varied between the two specified temperature–moisture combinations. Additionally, the temporal variations recorded during incubation underscore the necessity of monitoring GHG fluxes throughout the exposure period. Such temporal differences should be considered when assessing wetland carbon feedbacks.

### *4.2. Regulation of Greenhouse Gas Fluxes by Soil Carbon–Nitrogen Substrates and Extracellular Enzyme Activity*

Changes in soil carbon and nitrogen fractions were accompanied by contrasting extracellular enzyme responses under ELD and EHF (Figures 3 and 4) [40]. Under ELD, SOC and $NO_3^-$ concentrations remained relatively high, while $NH_4^+$ concentrations were generally lower than those under CK. Reduced microbial turnover and restricted substrate diffusion may have limited organic matter decomposition and nitrogen transformations, favoring the relative retention of carbon and nitrate. The decline in NOR activity at YA and EG was consistent with reduced activity of part of the denitrification pathway. However, the increase in sucrase activity at TF suggests that some carbon-degrading processes remained active despite the combined stress.

Under EHF, SOC concentrations declined, while $NH_4^+$ concentrations increased during the early incubation period and $NO_3^-$ concentrations initially increased before decreasing. These patterns are consistent with accelerated organic nitrogen mineralization and subsequent changes in nitrogen transformation pathways. Increased protease activity at RR and $N_2OR$ activity at TF and EG indicated substantial enzyme-level responses to EHF [18,32]. Nevertheless, changes in individual enzyme activities do not necessarily represent corresponding changes in whole reaction process rates.

$N_2O$ emissions may depend on the balance between its production and consumption rather than on the overall denitrification rate merely. In particular, differences between $NO_3^-$ reduction and the terminal reduction of $N_2O$ to $N_2$ may influence net $N_2O$ emissions [40–42]. The observed alterations in inorganic nitrogen pools, reductase activities, and $N_2O$ fluxes suggest that net $N_2O$ emissions may depend on the equilibrium between $N_2O$ production and reduction. However, since individual nitrogen transformation rates were not directly measured, this interpretation serves as a plausible explanation rather than a validated mechanism.

### *4.3. Microbial Community Reassembly and Functional Compensation Within Key Functional Groups*

Compound extreme weather events were associated with distinct changes in bacterial, fungal, and archaeal communities (Figures 5 and 6). Archaeal richness and diversity declined under EHF, whereas the bacterial and fungal communities showed more variable responses. Such differences indicate that microbial domains vary in their sensitivity to combined temperature and moisture stress [18,32,42]. Changes in taxonomic diversity may also differ from changes in microbial function because community turnover can alter the relative contributions of taxa with different metabolic capacities [41].

Under EHF, the enrichment of the methanogenic archaeon *Methanoculleus* was consistent with the observed increase in $CH_4$ fluxes during the middle incubation period. The enrichment of *Nitrososphaeraceae* also suggested changes in the composition of microorganisms associated with nitrogen cycling. Differentially enriched fungal taxa, including

*Aspergillus*, *Squamarina*, and *Cercospora*, may have contributed to changes in organic matter turnover, although their specific activities were not measured. Under ELD, the enrichment of *Haloferax* and *Candidatus Nitrosopumilus* suggested the persistence of halophilic and ammonia-oxidizing archaeal groups under combined cold and drought stress.

The relationships identified by RDA and PLS-PM further suggested that microbial community composition was associated with changes in soil properties and greenhouse gas emissions (Figures 8 and 9). Fungal communities showed a positive path coefficient with nitrogen cycling enzymes, whereas bacterial communities showed a negative association with carbon-cycling enzymes. These relationships are consistent with potential functional compensation among microbial groups, but taxonomic enrichment and modeled associations alone cannot establish functional redundancy or metabolic activity [43,44]. *Methanoculleus*, *Fusarium*, *Haloferax*, and *Candidatus Nitrosopumilus* may therefore be considered candidate biological indicators of responses to compound extreme weather events, subject to further functional validation.

### *4.4. Relationships Among Environmental Conditions, Microbial Communities, and Greenhouse Gas Fluxes*

The results of Mantel tests, RDA and PLS-PM suggested an interconnected pathway linking temperature and moisture conditions, soil carbon and nitrogen fractions, microbial communities, extracellular enzymes, and greenhouse gas emissions (Figure 7). Under EHF, associations between environmental factors and greenhouse gas fluxes were generally stronger than under ELD (Figure 7a,b). This pattern may reflect greater substrate availability and changes in microbial enzyme responses under warm, flooded conditions. The original statement that combined stress weakened substrate enzyme coupling appears to describe ELD treatment instead of EHF, and this interpretation requires confirmation before inclusion.

The PLS-PM results provided further evidence of associations among soil substrates, microbial communities, and enzyme activities. SOC was positively associated with bacterial communities, whereas soil nitrogen was positively associated with fungal communities. Negative associations were observed between soil carbon and nitrogen fractions and archaeal communities. Bacterial and fungal communities were also associated with carbon and nitrogen cycling as well as enzyme activities, respectively. These relationships support a multilevel conceptual framework for interpreting greenhouse gas responses, although the laboratory incubation design and path model do not establish causal relationships among all components [45].

From the management perspective, water level regulation and associated changes in redox conditions may influence methane production and nitrogen transformations. Monitoring SOC stability, inorganic nitrogen fractions, and microbial indicator taxa could improve the assessment of greenhouse gas emission risks, particularly when compound extreme weather event occurs [46]. This study presents several limitations concerning the spatial representativeness of its findings. First, the five sampling sites were selected purposively based on accessibility and habitat characteristics, rather than through random sampling throughout the Yellow River Delta. As a result, these sites represent specific sampling locations and should not be regarded as representative of the entire coastal wetland region or all corresponding habitat types. Second, soil samples collected at each site were pooled prior to incubation. Consequently, the three incubation replicates per treatment reflect within-site experimental replication rather than independent field replication. Therefore, the observed differences among sites should be interpreted within the context of these five selected locations. Future research should incorporate multiple independently sampled sites within each habitat type to enhance spatial representativeness and assess the broader applicability of these findings.

### *4.5. Limitations*

Several limitations of this study should be acknowledged when interpreting the results. First, the experiment was conducted under controlled laboratory incubation conditions, which exclude plant–soil feedbacks, soil fauna activity, diurnal temperature fluctuations and tidal hydrological dynamics that occur in natural wetlands. The closed serum vial system may also introduce bottle effects, such as gradual headspace gas accumulation and altered gas diffusion pathways, that differ from in situ field conditions. Our findings therefore reflect immediate biogeochemical responses to abrupt stress, and direct extrapolation to natural wetland ecosystems should be made with caution. Second, the 14-day incubation period captures the early and intermediate stages of flux response to extreme stress, but does not encompass longer-term microbial acclimation, community recovery or cumulative carbon and nitrogen turnover. Short-term pulsed emissions may not represent long-term net annual balances. Third, soil samples were collected from five habitat types selected via purposive sampling, and the limited number of sites restricts the spatial generalizability of results across the entire Yellow River Delta coastal wetland complex. Fourth, our experimental design includes only two combined temperature–moisture treatments and a control, without single-factor treatments of temperature or moisture alone. This prevents us from statistically disentangling the independent effects of each driver from their interactive effects, so the observed responses cannot be definitively attributed to compound extreme interactions. Finally, our microbial analyses rely on taxonomic marker gene sequencing rather than direct measurements of functional gene expression or in situ metabolic activity; the inferred functional roles of enriched taxa remain correlative and require independent validation.

### *4.6. Directions for Future Research*

Building on the findings and limitations of this study, four priority directions are proposed for future research. First, in situ manipulative field experiments should be combined with long-term monitoring of natural extreme weather events, to validate laboratory-derived response patterns under realistic field conditions with intact plant–soil systems and natural hydrological regimes. Second, extended time-series observations are needed that cover not only the immediate stress response phase but also the subsequent acclimation and recovery stages, to quantify the cumulative and long-term impacts of extreme events on wetland carbon and nitrogen budgets. Third, future work should integrate functional gene quantification, metatranscriptomics and stable isotope probing techniques to directly link shifts in microbial community composition to in situ metabolic activity, and to verify the functional contributions of candidate indicator taxa identified in this study. Fourth, full factorial experimental designs with single-factor temperature and moisture treatments should be adopted to explicitly separate additive and interactive effects of climatic drivers, which will provide more robust evidence for the ecological impacts of true compound extreme events. Expanding sampling coverage to encompass a broader range of habitat types and hydrological settings will also improve the generalizability of findings and support more reliable prediction of coastal wetland carbon feedbacks under future climate change.

## 5. Conclusions

The two predefined combined temperature–moisture treatments elicited divergent greenhouse gas flux responses in soils collected from five purposively selected sites in the eastern Yellow River Delta. These sites included an irrigation area (YA), tidal flat (TF), reed habitat (RG), *Salicornia* habitat (EG), and *Apocynum* habitat (RR). Under the ELD treatment, $CO_2$ and $CH_4$ fluxes were generally low; however, transient peaks in $N_2O$

emissions were observed alongside relatively higher levels of soil organic carbon (SOC) and nitrate. In contrast, the EHF treatment resulted in increased $CO_2$ fluxes, while $CH_4$ fluxes rose during the middle incubation period. This increase was accompanied by a more rapid decline in SOC and temporal variations in inorganic nitrogen fractions. The differing $N_2O$ responses may be linked to alterations in the balance between nitrate reduction and $N_2O$ reduction. Additionally, the two treatments were associated with changes in extracellular enzyme activities and microbial community composition. The observed enrichment of *Methanoculleus* under EHF and *Haloferax* and *Candidatus Nitrosopumilus* under ELD indicates that these taxa may function as potential indicators of microbial responses, pending functional validation. Correlation analyses and PLS-PM revealed associations among soil properties, microbial communities, enzyme activities, and greenhouse gas fluxes; however, these relationships do not confirm causal pathways. The findings are limited by the short duration of laboratory incubation, restricted sampling, and the purposive selection of five sites. The three replicates represented laboratory incubation replicates rather than independent field replicates; thus, the results should not be generalized to all coastal wetlands in the Yellow River Delta. Future research should incorporate factorial experiments with individual and combined treatments, multi-site field observations, isotope tracing, and microbial functional analyses to further explore these responses under natural conditions.

**Author Contributions:** Conceptualization, L.W.; Methodology, X.H.; Formal analysis, X.H. and G.Z.; Investigation, X.H., Q.M. and Q.C. (Qingliang Cui); Software, X.H. and Q.M.; Validation, C.L.; Resources, Z.C.; Writing—original draft preparation, X.H.; Writing—review and editing, L.W.; Project administration, G.Z.; Supervision, L.W. and Q.C. (Qingfeng Chen); Funding acquisition, L.W. and Q.C. (Qingfeng Chen). Author Q.C. (Qingfeng Chen) passed away prior to the publication of this manuscript. All other authors have read and agreed to the published version of this manuscript.

**Funding:** Shandong Provincial Natural Science Foundation for Young Scientists, ZR20240D201. Shandong Provincial Natural Science Foundation, ZR2025MS576). The National Natural Science Foundation of China, 42077051 and 42107316).

**Institutional Review Board Statement:** Not applicable.

**Informed Consent Statement:** Not applicable.

**Data Availability Statement:** The original contributions presented in this study are included in the article. Further inquiries can be directed to the corresponding authors.

**Acknowledgments:** All authors wish to express our deep gratitude to the editors and anonymous reviewers for the constructive feedback and valuable suggestions.

**Conflicts of Interest:** The authors declare that they have no known competing financial interests or personal relationships that could influence the work in this paper.

## References

1. Perkins-Kirkpatrick, S.E.; Lewis, S.C. Increasing trends in regional heatwaves. *Nat. Commun.* **2020**, *11*, 3357.
2. Sulikowska, A.; Wypych, A. Seasonal variability of trends in regional hot and warm temperature extremes in Europe. *Atmosphere* **2021**, *12*, 612. https://doi.org/10.3390/atmos12050612.
3. Wang, S.S.-Y.; Kim, H.; Coumou, D.; Yoon, J.-H. Consecutive extreme flooding and heat wave in Japan: Are they becoming a norm? Atmos. *Sci. Lett.* **2019**, *20*, e933. https://doi.org/10.1002/asl.933.
4. Imada, Y.; Watanabe, M.; Kawase, H.; Shiogama, H. The July 2018 high temperature event in Japan could not have happened without human-induced global warming. *SOLA* **2019**, *15A*, 8–12. https://doi.org/10.2151/sola.15A-002.

5. Codjoe, S.N.A.; Gough, K.V.; Wilby, R.L.; Kasei, R.; Yankson, P.W.K.; Amankwaa, E.F.; Abarike, M.A.; Atiglo, D.Y.; Kayaga, S.; Mensah, P.; et al. Impact of extreme weather conditions on healthcare provision in urban Ghana. *Soc. Sci. Med.* **2020**, *258*, 113072. https://doi.org/10.1016/j.socscimed.2020.113072.
6. Dong, S.; Sun, Y.; Aguilar, E.; Zhang, X.; Peterson, T.C.; Song, L.; Zhang, Y. Observed changes in temperature extremes over Asia and their attribution. *Clim. Dyn.* **2017**, *51*, 339–353. https://doi.org/10.1007/s00382-017-3927-z.
7. Smith, M.D. The ecological role of climate extremes: Current understanding and future prospects. *J. Ecol.* **2011**, *99*, 651–655. https://doi.org/10.1111/j.1365-2745.2011.01833.x.
8. Zhang, Y.; Guan, X.; Yu, H.; Xie, Y.; Jin, H. Contributions of radiative factors to enhanced dryland warming over East Asia. *J. Geophys. Res. Atmos.* **2017**, *122*, 7723–7736. https://doi.org/10.1002/2017JD026506.
9. Droppers, B. Multi-model hydrological reference dataset over continental Europe and an African basin. *Sci. Data* **2024**, *11*, 1009. https://doi.org/10.1038/s41597-024-03825-9.
10. Islam, S.U.; Hay, R.W.; Déry, S.J.; Booth, B.P. Modelling the impacts of climate change on riverine thermal regimes in western Canada's largest Pacific watershed. *Sci. Rep.* **2019**, *9*, 11398. https://doi.org/10.1038/s41598-019-47804-2.
11. Zhang, L.; Cai, C. Innovative measurement, trade-off-synergy relationship and influencing factors for agricultural net carbon emissions and effective supply of agricultural products in China. *Heliyon* **2024**, *10*, e24621. https://doi.org/10.1016/j.heliyon.2024.e24621.
12. Wu, H.; Su, X.; Singh, V.P. Increasing risks of future compound climate extremes with warming over global land masses. *Earth's Future* **2023**, *11*, e2022EF003466. https://doi.org/10.1029/2022EF003466.
13. Zscheischler, J.; Martius, O.; Westra, S.; Bevacqua, E. A typology of compound weather and climate events. *Nat. Rev. Earth Environ.* **2020**, *1*, 333–347. https://doi.org/10.1038/s43017-020-0060-z.
14. Hugelius, G.; Loisel, J.; Chadburn, S.; Jackson, R.B.; Jones, M.; MacDonald, G.; Marushchak, M.; Olefeldt, D.; Packalen, M.; Siewert, M.B.; et al. Large stocks of peatland carbon and nitrogen are vulnerable to permafrost thaw. *Proc. Natl. Acad. Sci. USA* **2020**, *117*, 20438–20446. https://doi.org/10.1073/pnas.1916387117.
15. Sun, J.; Xu, X.; Wang, Z.; Li, K.; Liu, C.; Li, C.; Cai, Z.; Zhao, X.; Xu, X.; Di, H.; et al. Effects of anthropogenic activities on soil microbial communities and greenhouse gas fluxes in coastal wetlands of the Yellow River Delta, China. *J. Environ. Sci.* **2026**, *161*, 176–188. https://doi.org/10.1016/j.jes.2025.08.066.
16. Lorrain-Soligon, L.; Robin, F.; Bertin, X.; Jankovic, M. Long-term trends of salinity in coastal wetlands: Effects of climate, extreme weather events, and sea water level. *Environ. Res.* **2023**, *237*, 116937. https://doi.org/10.1016/j.envres.2023.116937.
17. Capooci, M.; Barba, J.; Seyfferth, A.; Vargas, R. Experimental influence of storm-surge salinity on soil greenhouse gas emissions from a tidal salt marsh. *Sci. Total Environ.* **2019**, *686*, 1164–1172. https://doi.org/10.1016/j.scitotenv.2019.06.032.
18. Gao, D.; Gong, X.; Li, F.; Huang, Z.; Xu, A.; Yang, T.; Liang, H. Temperature dependency of methane emissions from alkaline wetlands under warming: Synergistic effects of soil properties and microbial communities. *Environ. Res.* **2025**, *286*, 123043. https://doi.org/10.1016/j.envres.2025.123043.
19. Tao, J.Y.; Liu, X.Y.; Chen, S. The responses of extracellular enzyme activities to saline conditions: A data synthesis. *Land Degrad. Dev.* **2026**, *37*, 2399–2410. https://doi.org/10.1002/ldr.70247.
20. Weng, Y.L.; Chen, R.; Hui, Y.; Chen, D.; Zhao, C.X. Boosting enzyme activity in enzyme metal-organic framework composites. *Chem. Bio Eng.* **2024**, *1*, 99–112. https://doi.org/10.1021/cbe.3c00091.
21. Zhao, L.; Shen, G.; Xu, T.; Wen, R.; Jiang, S. The preparation of titanium adipate and optimization of its catalytic ester exchange reaction for the synthesis of diisooctyl adipate. *RSC Adv.* **2025**, *15*, 6952–6961. https://doi.org/10.1039/d4ra08443h.
22. Li, S.; Zhou, M.; Guan, S.; Ma, L.; Zhu, S.; Wang, Y.; Chen, Y.; Sui, Y.; Jiao, X. Soil nitrogen-hydrolyzing enzyme activities respond differently to the freeze-thaw temperature and number of cycles. *Sci. Rep.* **2025**, *15*, 19026. https://doi.org/10.1038/s41598-025-98879-z.
23. Pitumpe Arachchige, P.S.; Hettiarachchi, G.M.; Rice, C.W.; Dynes, J.J.; Maurmann, L.; Wang, J.; Karunakaran, C.; Kilcoyne, A.L.D.; Attanayake, C.P.; Amado, T.J.C.; et al. Sub-micron level investigation reveals the inaccessibility of stabilized carbon in soil microaggregates. *Sci. Rep.* **2018**, *8*, 16810. https://doi.org/10.1038/s41598-018-34981-9.
24. Wang, Y.; Zhang, L.; Ma, X. Variation characteristics of extreme temperature indices in the Yellow River Delta region from 1994 to 2020. *Desert Oasis Meteorol.* **2025**, *19*, 170–178. https://doi.org/10.12057/j.issn.1002-0799.2304.28002.
25. Liu, J.; Lin, L.; Chen, X.Q.; Guan, Q.H. Characteristics of variation of precipitation time series in Yellow River Delta. *Water Resour. Prot.* **2012**, *28*, 22–28. (In Chinese)
26. Yan, Z.X.; Li, P.; Feng, C.H.; Cao, Y.X.; Lu, K.M.; Zhao, C.X.; Li, Z.B. Effects of riparian zone width and soil depth: Soil environmental factors drive changes in soil enzyme activity. *Land* **2025**, *14*, 2056. https://doi.org/10.3390/land14102056.

27. Velayutham, M.; Poncelet, M.; Enomoto, A.; Huffman, J.L.; Pandya, V.G.; Ichikawa, K.; Khramtsov, V.V.; Driesschaert, B. Line-shifting triarylmethyl radicals for imaging of enzyme activity using Overhauser-enhanced magnetic resonance imaging: Application to alkaline phosphatase. *Chem. Biomed. Imaging* **2025**, *3*, 35–44. https://doi.org/10.1021/cbmi.4c00059.
28. Limberis, J.D.; Nalyvayko, A.; Ernst, J.D.; Metcalfe, J.Z. A simple, single-tube overlapping amplicon-targeted Illumina sequencing assay. *PLoS ONE* **2023**, *18*, e0288687.
29. Pires, A.C.C.; Cleary, D.F.R.; Almeida, A.; Cunha, A.; Dealtry, S.; Mendonça-Hagler, L.C.S.; Smalla, K.; Gomes, N.C.M. Denaturing gradient gel electrophoresis and barcoded pyrosequencing reveal unprecedented archaeal diversity in mangrove sediment and rhizosphere samples. *Appl. Environ. Microbiol.* **2012**, *78*, 5520–5528. https://doi.org/10.1128/AEM.00386-12.
30. Chen, X.; Xue, D.; Wang, Y.; Qiu, Q.; Wu, L.; Wang, M.; Liu, J.; Chen, H. Variations in the archaeal community and associated methanogenesis in peat profiles of three typical peatland types in China. *Environ. Microbiome* **2023**, *18*, 48. https://doi.org/10.1186/s40793-023-00503-y.
31. Yang, Y.; Dou, Y.X.; Wang, B.R.; Xue, Z.J.; Wang, Y.Q.; An, S.S.; Chang, S.X. Deciphering factors driving soil microbial life-history strategies in restored grasslands. *iMeta* **2024**, *2*, e66.
32. Knight, C.G.; Nicolitch, O.; Griffiths, R.I.; Goodall, T.; Jones, B.; Weser, C.; Langridge, H.; Davison, J.; Dellavalle, A.; Eisenhauer, N.; et al. Soil microbiomes show consistent and predictable responses to extreme events. *Nature* **2024**, *630*, 690–696. https://doi.org/10.1038/s41586-024-08185-3.
33. Qu, Q.; Wang, Z.; Gan, Q.; Liu, R.; Xu, H. Impact of drought on soil microbial biomass and extracellular enzyme activity. *Front. Plant Sci.* **2023**, *14*, 1221288. https://doi.org/10.3389/fpls.2023.1221288.
34. Fernández, M.; Tapias, R. Seed dormancy and seedling ecophysiology reveal the ecological amplitude of the threatened endemism Picris willkommii (Schultz Bip.) Nyman (Asteraceae). *Plants* **2022**, *11*, 1981. https://doi.org/10.3390/plants11151981.
35. Pavankumar, T.; Mittal, P.; Hallsworth, J.E. Molecular insights into the ecology of a psychrotolerant Pseudomonas syringae. *Environ. Microbiol.* **2020**, *23*, 3665–3681. https://doi.org/10.1111/1462-2920.15304.
36. Song, Y.; Gao, X.; Wu, Y. Key metabolite differences between Korean pine (Pinus koraiensis) seeds with primary physiological dormancy and no-dormancy. *Front. Plant Sci.* **2021**, *12*, 767108. https://doi.org/10.3389/fpls.2021.767108.
37. Wang, Z.; Baskin, J.M.; Baskin, C.C.; Liu, G.; Ye, X.; Yang, X.; Huang, Z. Soil salinity regulates spatial-temporal heterogeneity of seed germination and seedbank persistence of an annual diaspore-trimorphic halophyte in northern China. *BMC Plant Biol.* **2024**, *24*, 604. https://doi.org/10.1186/s12870-024-05307-x.
38. Carissimo, A.; Comes, V.; Heussner, A.; Prime, A.-H. Enrichment of electrotrophic microorganisms from contrasting shallow-sea hydrothermal environments in bioelectrochemical reactors. *Front. Microbiol.* **2025**, *16*, 1539608. https://doi.org/10.3389/fmicb.2025.1539608.
39. Xu, S.; Wang, C.; Zhou, J.; Shan, H.; Li, B.; Shi, W.; Zhang, D.; Zhu, G.; Yang, X.; Wei, W.; et al. Impacts of land use on soil carbon, nitrogen, and phosphorus in the Eastern Qilian Mountains. *PLoS ONE* **2025**, *20*, e0326316. https://doi.org/10.1371/journal.pone.0326316.
40. Abed-alguni, B.H.; Alawad, N.A.; Al-Betar, M.A.; Paul, D. Opposition-based sine cosine optimizer utilizing refraction learning and variable neighborhood search for feature selection. *Appl. Intell.* **2022**, *53*, 13224–13260. https://doi.org/10.1007/s10489-022-04201-z.
41. Qu, Q.; Xu, H.; Ai, Z.; Wang, M.; Wang, G.; Liu, G.; Geissen, V.; Ritsema, C.J.; Xue, S. Impacts of extreme weather events on terrestrial carbon and nitrogen cycling: A global meta-analysis. *Environ. Pollut.* **2023**, *319*, 120996. https://doi.org/10.1016/j.envpol.2022.120996.
42. Pedron, R.; Esposito, A.; Cozza, W.; Paolazzi, M.; Cristofolini, M.; Segata, N.; Jousson, O. Microbiome characterization of alpine water springs for human consumption reveals site- and usage-specific microbial signatures. *Front. Microbiol.* **2022**, *13*, 946460. https://doi.org/10.3389/fmicb.2022.946460.
43. Sun, X.; Buchanan, P.J.; Zhang, I.H.; Zakem, E.J. Ecological dynamics explain modular denitrification in the ocean. *Proc. Natl. Acad. Sci. USA* **2024**, *121*, e2417421121. https://doi.org/10.1073/pnas.2417421121.
44. Afkhami, M.E.; Classen, A.T.; Dice, C.G.; Hernandez, D.J.; Li, V.W.; Rawstern, A.H.; Rudgers, J.A.; Stinchcombe, J.R.; Crawford, K.M. Unraveling complexity in climate change effects on beneficial plant–microbe interactions: Mechanisms, resilience, and future directions. *New Phytol.* **2025**, *249*, 93–113. https://doi.org/10.1111/nph.70644.
45. Zhang, X.; Li, Q.; Zhong, Z.; Huang, Z.; Bian, F.; Yang, C.; Wen, X. Changes in soil organic carbon fractions and fungal communities, subsequent to different management practices in Moso bamboo plantations. *J. Fungi* **2022**, *8*, 640. https://doi.org/10.3390/jof8060640.

46. Zscheischler, J.; Michalak, A.M.; Schwalm, C.; Mahecha, M.D.; Huntzinger, D.N.; Reichstein, M. Impact of large-scale climate extremes on biospheric carbon fluxes: An intercomparison based on MsTMIP data. *Glob. Biogeochem. Cycles* **2014**, *28*, 585–600. https://doi.org/10.1002/2014GB004826.

**Disclaimer/Publisher's Note:** The statements, opinions and data contained in all publications are solely those of the individual author(s) and contributor(s) and not of MDPI and/or the editor(s). MDPI and/or the editor(s) disclaim responsibility for any injury to people or property resulting from any ideas, methods, instructions or products referred to in the content.